Performance Comparison of NN based PI and Fractional Order SMC for Sensorless Speed Control of IPMSM Drive

Ashraf Hagras[1]

Abstract: This paper investigates the performance of Neural Network (NN) based PI Controller (NNC) and Fractional Order Sliding Mode Controller (FOSMC) for sensorless speed control of Interior Permanent Magnet Synchronous Motor (IPMSM). It proposed new method of NN based PI sensorless speed control based on offline learning using look up table obtained from analysis of the PI controller. The FOSMC was designed, analysed and its stability was guaranteed using Lyapunov stability theory to validate its higher performance. This paper proposes novel speed observer as low pass filter of motor currents and load torque in the time domain to increase the reliability of the closed loop system. Simulations results using MATLAB/SIMULINK proved the improved performance of the two controllers and the strong robust performance of FOSMC compared to Neural Network based PI sensorless speed Controller (NNC) against large ranges of uncertainties and external load disturbances in field-oriented Vector Control (VC) scheme. Analysis study of the effect of fractional order differentiator was presented to show that as its value decreases, the transient and steady state performance of the motor is improved.

1. Introduction

Permanent magnet synchronous motor is the main motor used in many systems such as Wind Energy Conversion Systems (WECS), Electric Vehicle Systems (EVS) and robotic applications because it has many advantages like high torque per weight, absence of dc excitation and high efficiency. Since its nonlinear model, its sensitivity to external disturbances like load torque and model parameters variations like its stator resistance and inductance will affect its performance. Also, other various operating conditions like temperature, skin effect and saturation can affect its performance. This attracts many advanced control methodologies to improve the performance of the drive such as sliding

---

[1] Assist. Prof., Department of Eng. and Scientific Apparatus, Egyptian Atomic Energy Authority, Egypt. ashrafa1973@yahoo.com

mode control, nonlinear backstepping control, fuzzy logic control and neural network controllers. Sliding mode control is simple, accurate and robust and proved its strong robustness against other nonlinear strategies. It has two main drawbacks: the chattering phenomenon and the reaching phase. To eliminate the chattering and speed the reaching phase, High Order Sliding Mode Control (HOSMC) like Second Order Sliding Mode Control (SOSMC) was proposed. But the tuning of its Parameters represent an obstacle to achieve improved performance compared to 1st order SMC and the uncertainties and parasitic present in the system states support this obstacle [2, 10].

Also, Super Twisting SMC (STSMC) was proposed which is a different form of HOSMC can't overcome the disturbances which grow in time and requires the known of their bounds in addition to their adaptive gain tuning [5, 10, 11]. A derivative free Kalman filter was proposed in [12] to estimate the unknown disturbances and avoid heavy parameters tuning. Also, the adaptive gain was optimized using Rooted Tree Optimization (RTO) algorithm [13]. Ref. [9] utilized improved modified sliding surface to compensate the nonlinearities increase and the mismatched uncertainties. In this paper, another law of SMC is FOSMC which provide continuous output and more degree of freedom than integer one. This advantage motivates the PMSM to provide precise speed control and compensation of parameters variation and external disturbances. The fractional order SMC is based on fractional order sliding surface [1-3] and based on fractional PID sliding surface [4-5]. Moreover, the sliding mode surface is based on nonsingular fast terminal sliding surface [6], on nonsingular terminal sliding surface [7] or on nonlinear integral sliding surface [8]. In addition, each strategy in the previous literature has different switching law with its complexities and more parameters. In this paper, FOSMC used is based on 1st order sliding mode surface compared to the previous literature to avoid complexities and parameters tuning difficulties of the controller. In addition, it is used in the speed loop without adaptive law to improve the transient speed and torque response compared to [1] where it is used in the current loop. In regard to the literature, FOSMC was used in addition to Estimator or observer [5], filter [14], adaptive mechanism [1] or another controller [15] to improve the performance of the system.

Basically, NN can be trained in online or offline mode. Online training means changing the weights and the biases of the NN continuously during the control process tell get the desired input. This makes it attractive because it can compensate system parameters variations and adapt with changing operating conditions. But this adds to the computational burden of the processor and requires very fast processor to accomplish this process [16]. Back propagation is the preferred training algorithm for feed forward neural networks. Offline training can be achieved using patterns of data obtained from analysis of simulation of the PI controller. The weights are fixed after implementing the NN. Because the calculations include only addition, multiplication, and sigmoidal function, it can be implemented easily using simple hardware or on any processor and provide fast response. It takes the error integral information as the input, which minimizes the steady state error of speed tracking. A selected feed forward NN is trained to model this controller using back propagation algorithm. After offline training, the NN is used to control the speed of PMSM [17-21]. This paper is arranged as follows: sensorless speed control of IPMSM and its MTPA are modelled in section 2. Sections 3 and 4 provide the design of NNC and FOSMC respectively. FOSMC is digitally discretized in section 5 and the simulation results were presented in section 6. The conclusions were drawn in section 7.

2. Mathematical Modeling of Sensorless speed control of IPMSM and MTPA

The electrical model of Interior PMSM (IPMSM) in the rotor rotating reference frame can be described as follows:

$$L_d \frac{di_d}{dt} = -Ri_d + \omega_r L_q i_q + v_d$$
$$L_q \frac{di_q}{dt} = -Ri_q - \omega_r L_d i_d - \omega_r \lambda_f + v_q \tag{1}$$

Where v_d and v_q are the stator d and q axis stator voltages respectively, R is the stator resistance, L_d and L_q are the d and q axis stator inductances, λ_f is the permanent magnet flux and ω_r is the electrical rotating speed and is defined as: $\omega_r = P\omega_m$, ω_m is the rotor angular velocity.

Based on (1), the control voltage v_d and v_q can be derived by regulating the errors in the d and q axis stator currents neglecting the coupling terms $\omega_r L_q i_q$ and $(\omega_r L_d i_d + \omega_r \lambda_f)$ to achieve independent control of i_d and i_q in the inner current loops and consequently the torque and flux as depicted in Figs. 2 and 4. For IPMSM, the electromagnetic torque can be expressed as:

$$T_e = \frac{3P}{2}\left(\lambda_f i_q + (L_d - L_q)i_d i_q\right) = k_t i_q + \frac{3P}{2}(L_d - L_q)i_d i_q \tag{2}$$

P is the number of pole pairs and k_t is the torque constant.

The mechanical equation which governs the IPMSM can be described as follows:

$$T_e = J\frac{d\omega_m}{dt} + B\omega_m + T_L \tag{3}$$

J is the rotor moment of inertia; B is the viscous friction coefficient and T_L represents the applied load torque disturbance.

Equating Eqs. (2) and (3) and performing some arrangements, we can obtain:

$$\omega_{est} = \left.\left(\left[(k_t/J) + (3P/2J)(L_d - L_q)i_d\right]i_q - T_L/J\right)\right/ s + J/B \tag{4}$$
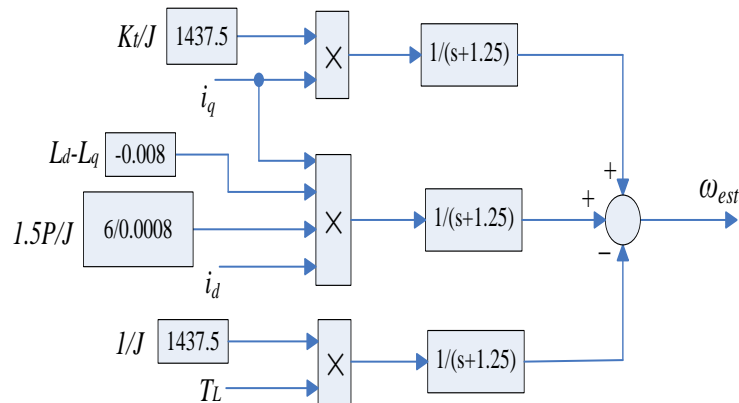

Fig. 1 The B. D. of the speed observer

This is the speed observer equation where the speed is function of i_d and i_q only or low pass filter of these currents and the load torque. Fig. 1 shows the Block Diagram (B. D.) of speed observer according to Eq. (4). This low pass filter can be realized mathematically as carried out in this paper or searched online with reference to the cut off frequency independent of the electrical parameters or the permanent magnet flux. This observer proved its robust performance as will be shown in section 6.1.2 at high and low speeds. This model does not use adaptive model to decrease the computational burden of the processor [28, 29]. Maximum Torque Per Ampere (MTPA) strategy can be employed to increase the maximum torque/current ratio and the efficiency of the IPMSM drive in the constant torque region below the rated speed. MTPA can be obtained in three ways; mathematical modeling based MTPA, look-up table and signal injection based MTPA. In such technique, the reference i_d can be evaluated by differentiating the torque with respect to the current to obtain:

$$i_d^* = \left. \left(-\lambda_f + \sqrt{\lambda_f + 4(L_d - L_q)^2 i_q{}^2} \right) \middle/ 2(L_d - L_q) \right.$$

(5)

For successful application of MTPA control, this relation can be approximated by Taylor's series expansion around zero to obtain the following:

$$i_d^* = \frac{\lambda_f}{2(L_q - L_d)} - \frac{\lambda_f}{2(L_q - L_d)} \left[\begin{array}{l} 1 + \dfrac{2(L_q - L_d)^2}{\lambda^2{}_f} i^2{}_q \\[2ex] + \text{higher orders of } \dfrac{4(L_q - L_d)^2}{\lambda^2{}_f} i^2{}_q \end{array} \right]$$

This relation can be approximated by neglecting its higher orders as follows:

$$i_d^* = \left[(L_d - L_q) / \lambda_f \right] i_q^2$$

(6)

Replacing i_d from Eq. (5) into Eq. (2) results the following [30-31]:

$$T_e = \frac{3P}{4} \left(\sqrt{\lambda_f{}^2 + 4(L_d - L_q)^2 i_q{}^2} + \lambda_f \right) i_q \cong \frac{3P}{2} \lambda_f i_q = f(i_q)$$

As shown, the second term under the square root can be neglected compared to the first term **.**

3. Neural Network based PI Controller (NNC)

The NN based PI controller was designed with new method which depends on offline data gathered from the analysis of operation of the PI controller. The PI controller was simulated in single model with two inputs and registering the output. These data were used as look up table of 64 samples for offline learning of NN. The NN was designed using (nntool) order of MATLAB toolbox (2018). Therefore, this NN was trained using the Levenberg–Marquardt training algorithm under NN toolbox. The inputs of NN were the inputs of PI controller that are the error and its time change. Therefore,

The NN was implemented with single hidden layer of ten neurons and tan-sigmoid is its activation function. Where the activation function of the output layer is linear function. Fig. 3 presents the B. D. of the NN based PI speed controller based on FOC [27].
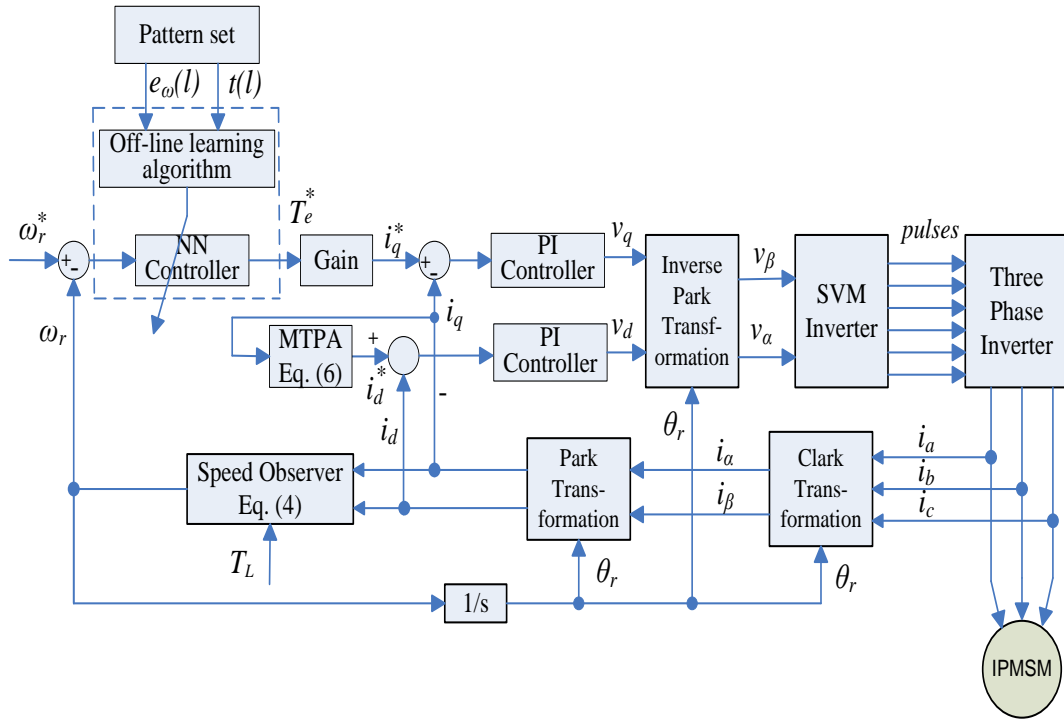

Fig. 2: The B. D. of IPMSM sensorless speed control based NN controller.

4. Design and stability analysis of Fractional Order Sliding Mode Controller (FOSMC)

In this design, a first order sliding surface is chosen to avoid tuning complexities of the controller parameters:

$$S = e = \omega_{\text{ref}} - \omega_r$$

When the sliding mode occurs on the sliding surface:

$$S = \dot{S} = \dot{e} = \dot{\omega}_{\text{ref}} - \dot{\omega}_r = -\frac{3P\lambda_f}{2J}i_q - \frac{3}{2}P\frac{(L_d - L_q)}{J}i_d i_q + \frac{B}{J}\omega_r + \frac{1}{J}T_L = 0 \qquad (7)$$
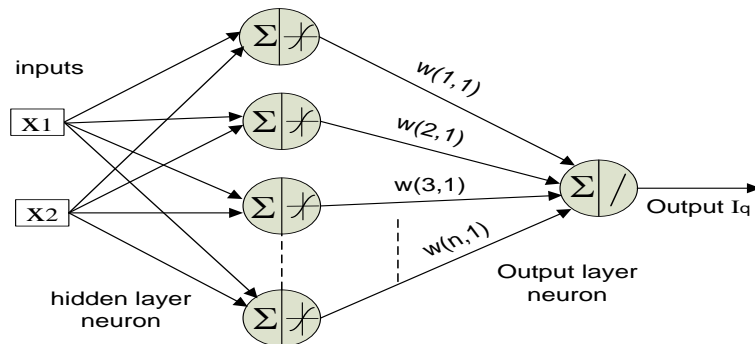

Fig. 3: The structure of BPNN

As a result, the equivalent control current i_q can be obtained by $S=0$:

$$u_{eq} = \frac{2}{3P[\lambda_f + (L_d - L_q)i_d]}(B\omega_r + T_L)$$

To guarantee the reaching condition of the proposed switching manifold, the control output should make the initial state converges to sliding manifold. Therefore, we choose the switching control law as follows:

$$\dot{S} = -KD^r sgn(S), \quad 0 < r < 1, K > 0 \tag{8}$$

Where r is the order of the fractional order derivative of the signum function. Therefore, we choose the Lyapunov function candidate as follows: $V = (1/2)S^2$, Taking the derivative of V with respect to time yields:

$$\dot{V} = S\dot{S} = -SKD^r sgn(S) + \frac{S}{J}(-\frac{3P}{2}\lambda_f i_q - \frac{3}{2}P(Ld - Lq)i_d i_q + B\omega_r + T_L + JKD^r sgn(S)) \tag{9}$$

To guarantee the asymptotic stability: $\dot{V} < 0$, now we can propose the control law as follows:

$$i_q^* = \frac{2}{3P[\lambda_f + (Ld - Lq)id]}(B\omega_r + T_L + JKD^r sgn(S)) \tag{10}$$

Substituting (10) into (9) results:

$$\dot{V} = S\dot{S} = -SKD^r sgn(S) < 0 \text{ for } K > 0$$

Then, global asymptotical stability is ensured, and the speed control tracking is achieved without dependence on motor parameters. Fig. 4 shows the block diagram of sensorless speed control based FOSMC.
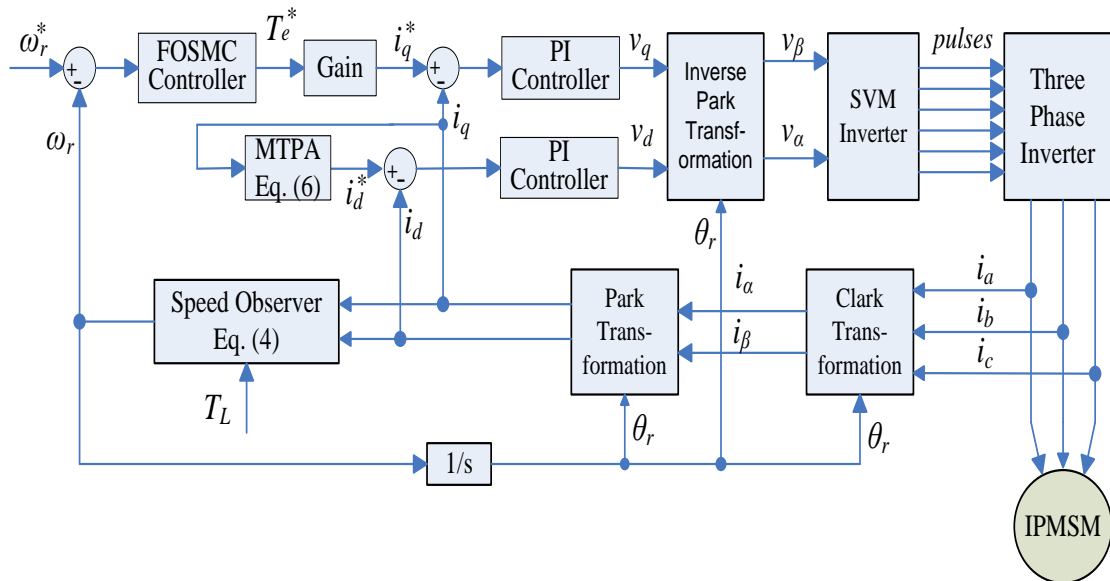

Fig. 4: The B. D. of IPMSM sensorless speed control based FOSMC.

5. Digital Discretization of fractional order derivative operator

Continuous time estimation of fractional integration and differentiation can be expressed as follows: continuous methods as follows; Carlson's method, Matsuda's method, oustaloup method and Chareff's method. While discrete time estimation can be expressed as follows; the backward Euler and PSE or backward Euler and CFE or trapezoidal rule and CFE [22]. There are three rules that permit to take the derivative of noninteger functions many times in the time domain: the Grunwald- Letnikov (GL), the Riemann-Liuville (RL) and the Caputo fractional definitions. Any non-integer can be expressed as the (fractional) order fundamental operator $_a D_t^r$, where a and t are the limits and $(r \in R)$ is the order of the operation.

Therefore, the fractional operator in the time domain can be evaluated by; the Grunwald- Letnikov (GL), the Riemann-Liuville (RL) and the Caputo fractional. The Laplace transform of the fractional differentiator or integrator of zero initial conditions for the GL or RL methods (for order r) is defined by:

$$L\left\{_a D_t^{\pm r} f(t); s\right\} = s^{\pm r} F(s)$$

To can implement this function easily, the fractional-order operator s^α (α is a real number) can be expressed by the following generating function $s = \omega (z^{-1})$. The three most known discretization rules are the trapezoidal (Tustin) rule, the backward difference (Euler) rule, and the Al-Alaoui operator. The generating function can be used in the following formula:

$$\omega(z^{-1}) = \frac{1}{\beta T}\frac{1-z^{-1}}{\gamma+(1-\gamma)z^{-1}} \tag{11}$$

Where β and γ are the gain and phase tuning parameters, respectively. For example, when $\beta = 1$ and $\gamma = \{0, 1/2, 7/8, 1, 3/2\}$, the generating function (11) will be the forward Euler, the Tustin, the Al-Alaoui, the backward Euler, and the implicit Adams rules, respectively.

The two methods used for evaluating the digital estimation of the generating function are as follows:
1- Power Series Expansion (PSE) have polynomials which have only zeros and can constitute FIR filter.
2- CFE is a rational transfer function (IIR filter) has poles and zeros [23]. But estimation of rational functions converges faster and in larger domain in the complex plane. This estimated transfer function can be implemented easily with any processor like D.S.P.

Therefore, in our paper, the transfer function was discretized based on the Aouli (which is mixed of the Euler rule and the Trapezoidal rule) and CFE discretization scheme. This method has better estimation in the high frequency range than that the Tustin rule [24]. Therefore, the generating function for discretization will be:

$$(\omega(z^{-1}))^{\pm r} = (\frac{8}{7T}\frac{1-z^{-1}}{1+z^{-1}/7})^{\pm r} \tag{12}$$

CFE can be used to approximate the function (12) which is an infinite order of rational discrete transfer function to finite order rational one.

$$(\omega(z^{-1}))^{\pm r} = \left(\frac{1+a}{T}\right)^{\pm r} \text{CFE}\left\{\left(\frac{1-z^{-1}}{1+az^{-1}}\right)^{\pm r}\right\}_{p,q}$$

$$= \left(\frac{1+a}{T}\right)^{\pm r} \frac{P_p(z^{-1})}{Q_q(z^{-1})} = \left(\frac{1+a}{T}\right)^{\pm r} \frac{p_0+p_1 z^{-1}+....+p_m z^{-p}}{q_0+q_1 z^{-1}+....+q_m z^{-q}} \quad (13)$$

Where *CFE{u}* denotes the continued fraction expansion of *u*; *p* and *q* are the orders of the approximation and *P* and *Q* are polynomial functions of degrees *p* and *q*. Normally, we can set $p = q = n$. Coefficients of *P* and *Q* polynomials depend on the order of the estimated model and canbe calculated from the following forms for $p = q = 1$. The value of approximation order *n* can be truncated to n > 1, but we avoided the complexity of design of the controller. The weighting factor *a* was chosen = 1. Assume sampling period T = 0.001 s. We have the following approximation of the fractional order derivative [25-27]:

$$p_0 = q_0 = \frac{2}{a+r+\text{ra}-1}, \quad p_1 = \frac{a-r-\text{ar}-1}{a+r+\text{ra}-1}, \quad q_1 = 1$$

6. Simulation Results and Discussions

To validate the improved response of the two controllers, they were simulated using MATLAB/SIMULINK. The improved responses of the two controllers were ensured by testing the two controllers under various operating conditions. The comparison of the two controllers was achieved to ensure the superior performance and strong robustness of the proposed controller FOSMC compared to NNC against parameters uncertainties and external disturbances. Fig. 5 depicts the block diagram of the proposed system based FOSMC using MATLAB/SIMULINK. The IPMSM parameters are as follows: R=2.875 Ω, $L_{D=}$8 mH, L_q=16 mH, B (the viscous friction coefficient) = 0.001 N. m. s, J (the moment of inertia) = 0.0008 kg m^2, P (the number of pole pairs) = 4. The flux linkage= 0.19167 V.s. The current control employs space vector Pulse Width Modulation (SVPWM) strategy to generate the six pulses for the 2-level three phase inverter and the switching frequency of the inverter is constant at 20 kHz. The B. D. of SVPWM based current control is shown in Fig. 6 The simulation results ensure the comparison under three conditions:

  6.1) During normal operation.
  6.2) 100% uncertainties of R, L_d and L_q.
  6.3) -50% uncertainties of R, L_d and L_q.
In addition, the fractional order differentiator (*r*) was varied to show its effect on the transient speed and torque performance.

Fig. 5 The B. D. of the proposed system using MATLAB/SIMULINK

Fig. 6 The SVPWM current control using MATLAB/SIMULINK

6.1 During Normal operation

6.1.1 Start-up response

Figure 7 shows the torque start up response of the two controllers. The NNC has a faster response but with higher overshoot and lower undershoot than the FOSMC. The FOSMC has peak overshoot doesn't exceed 15 N.m. compared to the NNC which reaches 21 N.m. Fig. 8 depicts faster speed response for NNC but FOSMC has lower overshoot and lower steady state speed error (0.5 r/s) than NNC (0.8r/s).

6.1.2 Step load change and torque ripples

Figure 9 illustrates the step load change response at t=0.2 ms. The FOSMC has torque faster response, but it rather has higher overshoot than NNC. The two controllers have comparable performance in Fig. 10 where the step load change has no effect on the speed response. As shown, the torque ripples don't exceed 0.15 N.m. at T=6 N.m or less. As illustrated in Fig. 11 and 12, both controllers have robust performance at low speeds (10r/s) with the same inherent steady state error (0.5 r/s for FOSMC

and 0.8 for NNC) at high speeds. Accordingly, the torque ripples were decreased to less than 0.05 N.m for both. It is shown that the FOSMC has lower speed overshoot than the NNC. Therefore, the FOSMC has stronger robust performance than NNC at normal operation and against load disturbance.
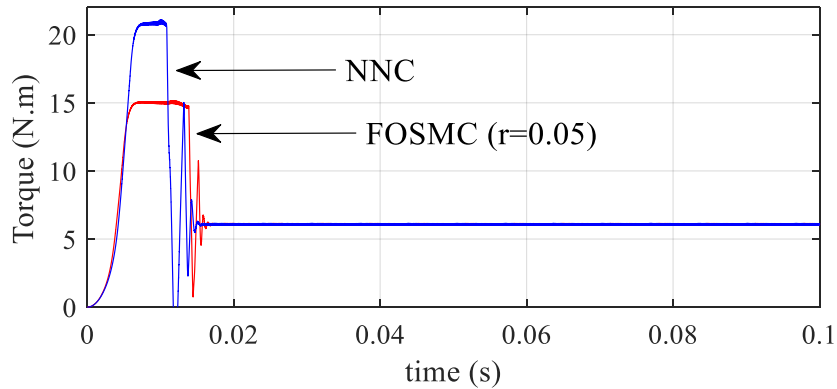
Fig. 7: The torque start up response of the two controllers.
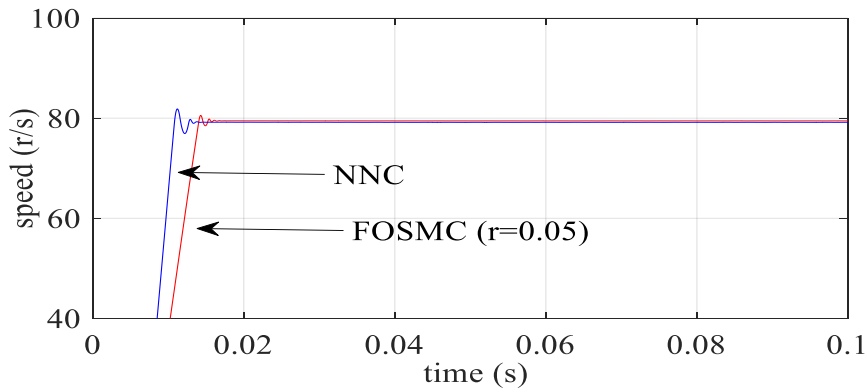
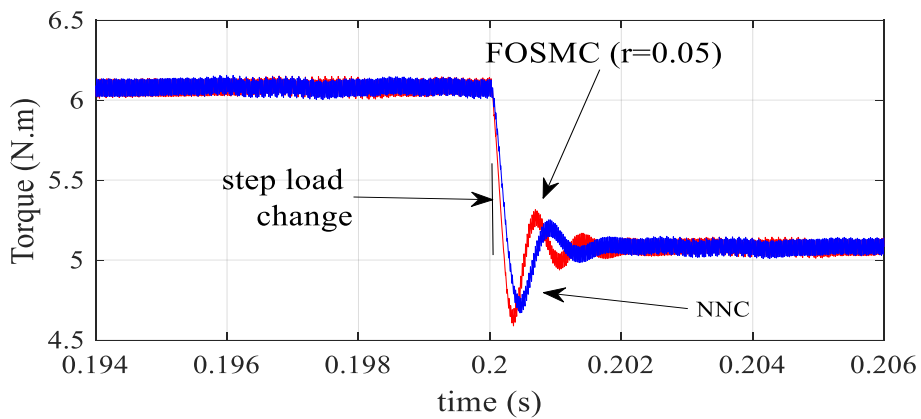Fig. 8: The speed start up response of the two controllers

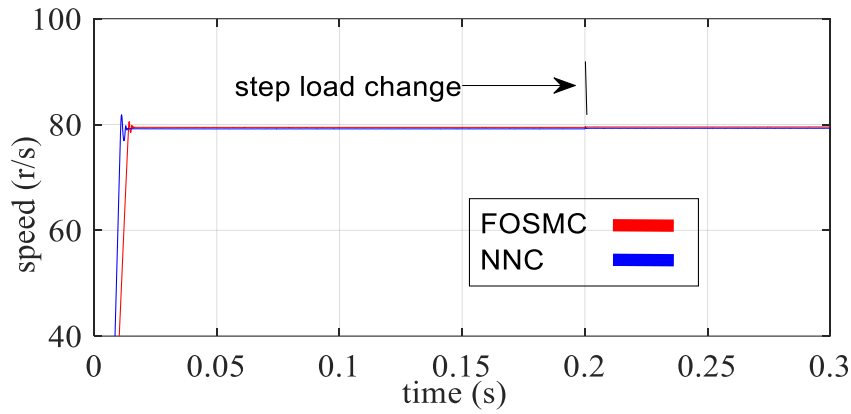

Fig. 9: The step load change response at normal operation

Fig. 10 The speed response of step load change
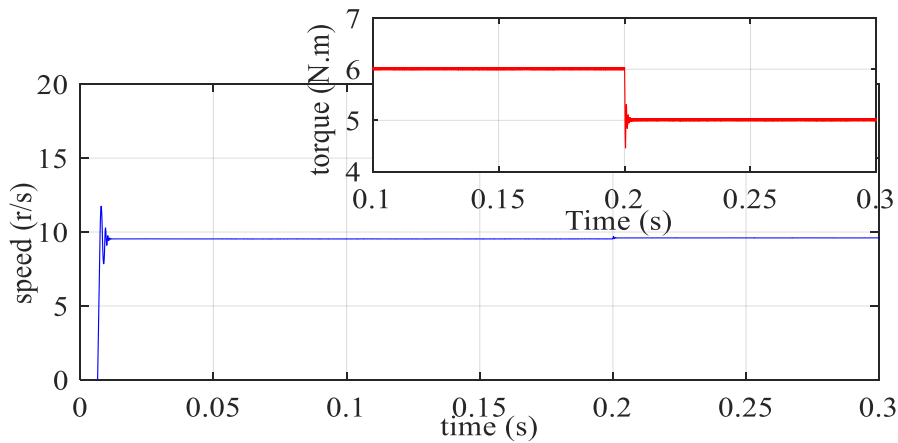
Fig. 11: The speed and torque response of FOSMC based speed controller at low speed
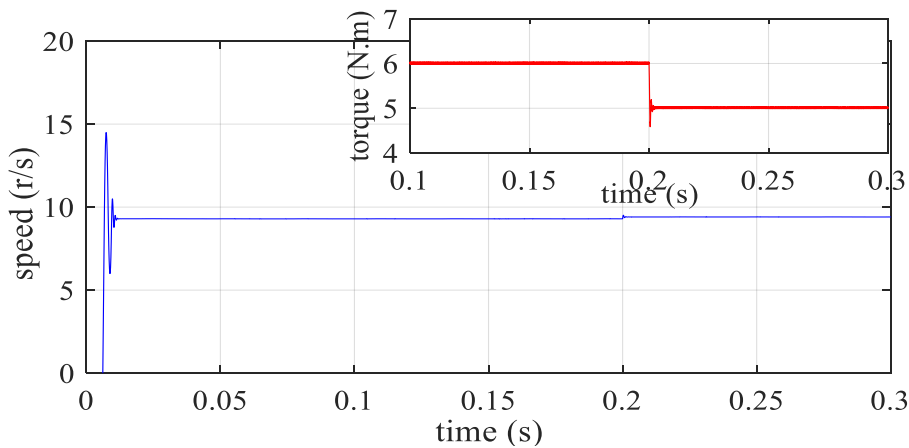
Fig. 12: The speed and torque response of NN based speed controller at low speed

6.2 Compensation of 100% uncertainties of *R, L_d* and *L_q*

In this test, we set IPMSM parameters with 100% uncertainties as follows: R=5.75 Ω, L_D=16 mH and L_q=32 mH.

6.2.1 Startup Response

As depicted in Fig. 13, the proposed two controllers have robust speed start up performance. But the FOSMC have stronger robust steady state performance with lower steady state error 0.52 (r/s)

compared to 0.8 (r/s) of the NNC. Also, FOSMC have lower peak speed overshoot 2 (r/s) above the desired speed compared to 7 (r/s) of the NNC.

Fig. 14 shows that The NNC has higher torque start up overshoot and lower undershoot than the FOSMC and both have the same settling time. This means that the start-up torque for 100% uncertainties maybe harmful to the motor in case of NNC.
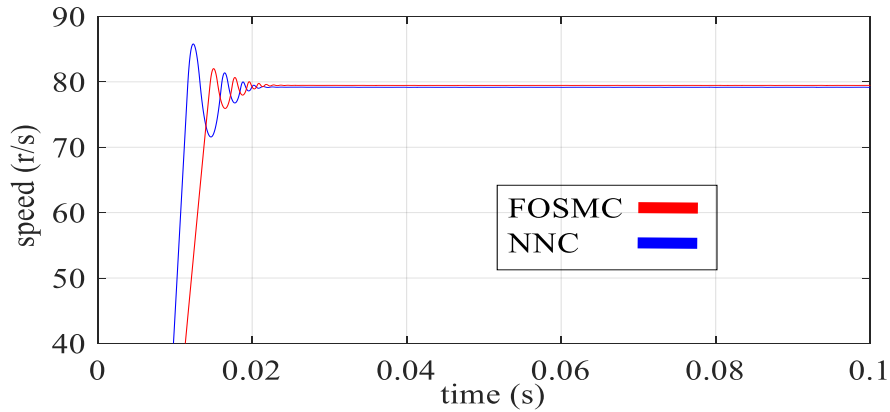

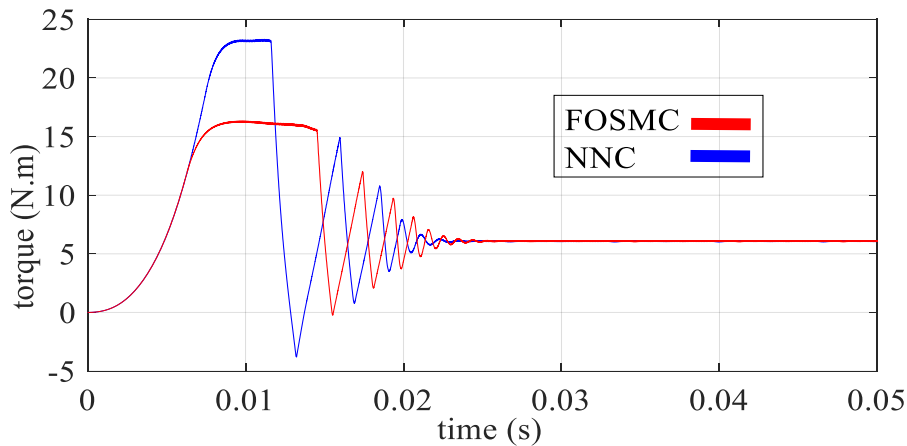Fig. 13: The speed start up response of the two controllers for 100 % uncertainties

Fig. 14: The torque start up response of the two controllers for 100 % uncertainties

6.2.2. Step Load Change

Figure 15 illustrates the torque response of the two controllers during load torque step change. The two controllers have comparable torque performance. But the proposed FOSMC responds fast with rise time less than 1 ms but with larger overshoot. Fig. 16 depicts that the two controllers have robust speed performance against step load change. The FOSMC has rather small overshoot. This means that FOSMC have also stronger robust performance against 100% parameters uncertainties and external load disturbance.

6.2.3. Torque Ripples

Figure 15 illustrates the torque ripples of the two controllers. They have comparable amounts of torque ripples doesn't exceed 0.15 N.m.

6.3. Compensation of -50% uncertainties of R, L_D and L_q

In this test, we set the motor parameters with -50% uncertainties as follows: R=1.3 Ω, L_D =4 mH and L_q =8 mH.

6.3.1 Start up response

As shown in Fig. 17, NNC has faster speed response than FOSMC but has rather higher steady state error. While in Fig. 18, NNC has higher overshoot and lower torque undershoot than FOSMC and this is safe at start up because the high oscillations may be harmful for the motor. Therefore, FOSMC has better adaptive capability than NNC in all cases of uncertainties.
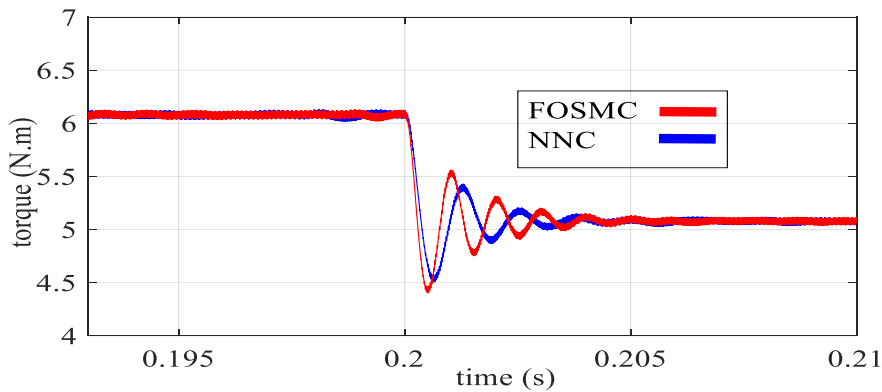
Fig. 15 The torque response of step load change for 100% uncertainties.
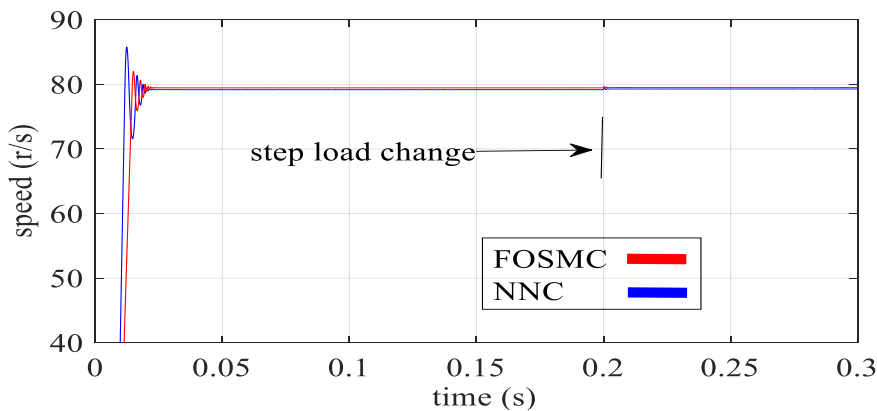

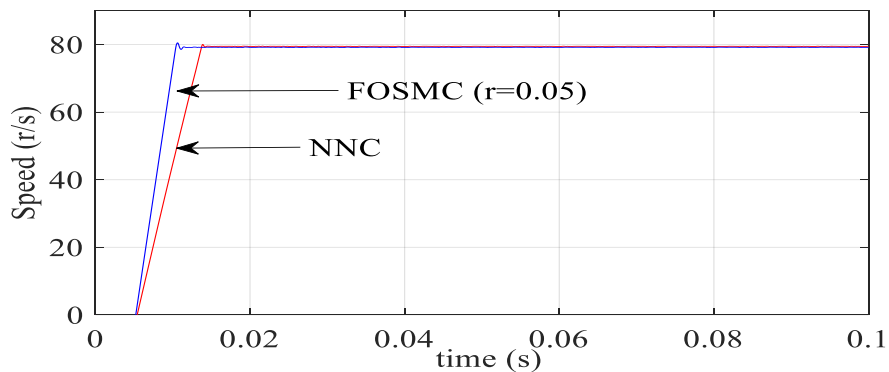Fig. 16 The speed response of step load change for 100% uncertainties

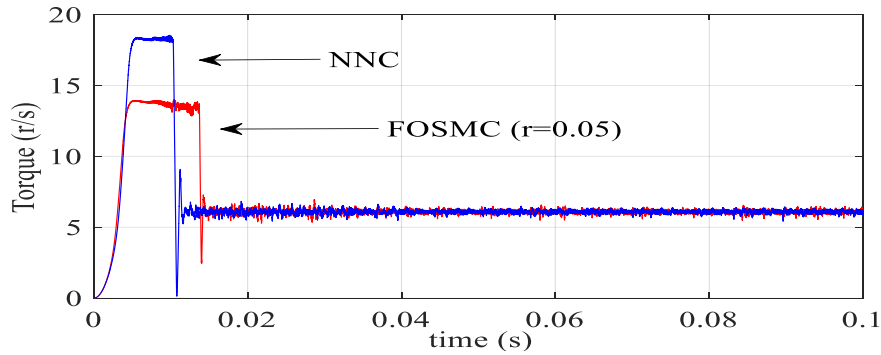Fig. 17 The speed start up response for -50% uncertainties

Fig. 18 The torque start up response for -50% uncertainties

6.3.2 Step load change

As illustrated in Figs. 19 and 20, when the load is suddenly decreased from 6 N.m to 5 N.m at t=0.2 s, the two controllers have comparable transient and steady state speed and torque performance although the FOSMC has lower overshoot and steady state speed error. They also have comparable amounts of ripples 0.٧ N. m. as shown in Fig. 20.
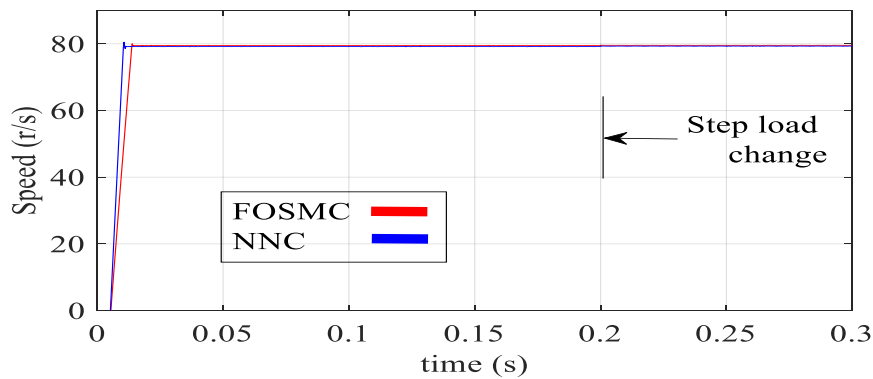

Fig. 19 The speed response of step load change for -50% uncertainties
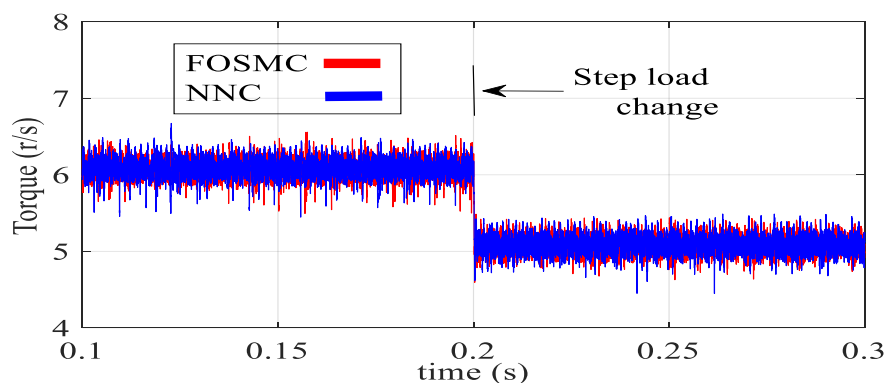

Fig. 20 The torque response of step load change for -50% uncertainties

6.4. The effect of fractional order differentiator (r) value

6.4.1 Torque response

As shown in Fig. 21, the lowest torque overshoot is for r=0.05 and the highest overshoot is for r =0.2. It can be concluded as *r* increases, the start up torque overshoot increases and the settling time

increases and reaches more than 30 ms for (r= 0.2) compared to 15 ms for (r=0.05 and 0.1). Also, in Fig. 22, the torque step response for r=0.2 has the highest overshoot and excessive oscillations for 4 ms and these oscillations decrease as (r) decrease.

6.4.2. Speed response

Fig. 23 depicts the speed response of varying the fractional order differentiator value. The speed response for r=0.05 has the lowest overshoot and smaller settling time. Therefore, as r increases, the steady state speed error decrease and the overshoot increases as shown in Fig. 24 where the steady state speed errors as follows: e_{ss} (r=0.2) =0.07 r/s, e_{ss} (r=0.1) =0.37 r/s, e_{ss} (r=0.05) =0.543 r/s and e_{ss} (r=0) =0.478 r/s.
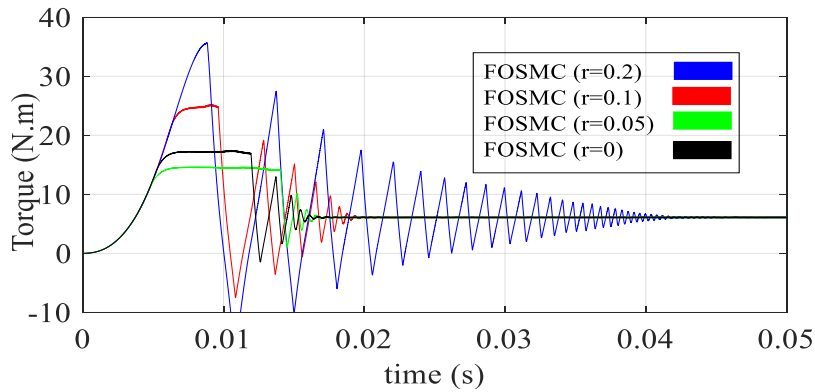

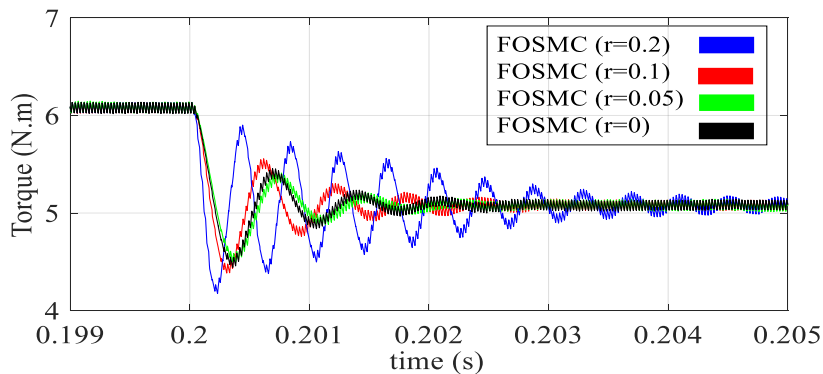Fig. 21 The effect of (r) on the start up torque response
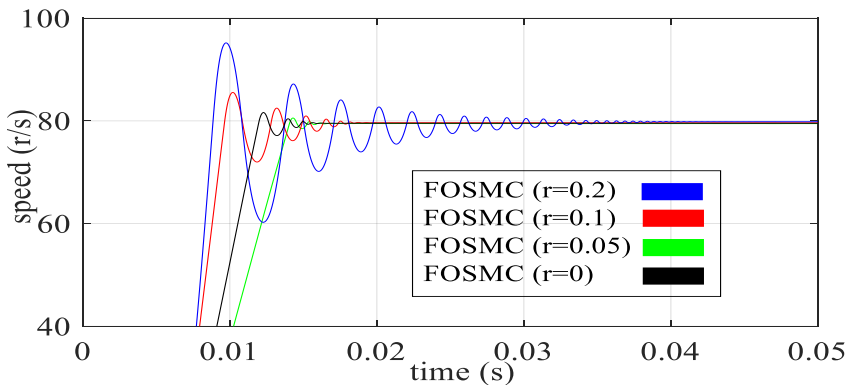

Fig. 22: The effect of (r) on the step torque response

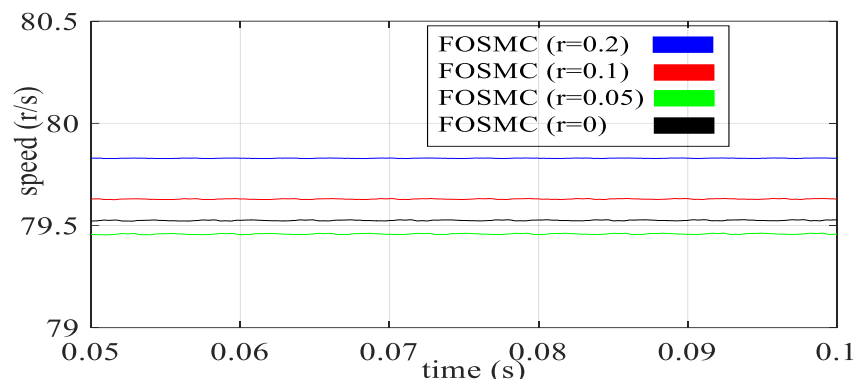Fig. 23: The effect of (r) on the speed start up response

Fig. 24: The effect of the fractional order differentiator (r) on the steady state speed

7. Conclusions

The NN based PI speed controller was designed accurately based on offline learning from pattern of 64 samples. The FOSMC based speed controller was designed, discretized and its stability was guaranteed using Lypunov stability theory. The NNC and FOSMC proved their improved response during normal operation and against external disturbances and large measurement uncertainties. But FOSMC based speed controller proved its stronger robust transient and steady state speed and torque performance against large range uncertainties and external load disturbances. The fractional order differentiator proved that as it decreases, the transient speed and torque performance is improved with smaller overshoot and smaller settling time.

References

[1] Sayed Hamed Hosseini and Mohammad Tabatabaei, "IPMSM velocity and current control using MTPA based adaptive fractional order sliding mode controller", *Engineering Science and Technology, an International Journal*, vol. 20, pp. 896-908, 2017.

[2] BiTao Zhang, YouGuo Pi and Ying Luo, "Fractional order sliding-mode control based on parameters auto-tuning for velocity control of permanent magnet synchronous motor", *ISA Transactions*, vol. 51, pp. 649-656, 2012.

[3] Nasim Ullah, Muhammad Asghar Ali, Asier Ibeas and Jorge Herrera, "Adaptive Fractional Order Terminal Sliding Mode Control of a Doubly Fed Induction Generator-Based Wind Energy System", *IEEE Access*, vol. 5, pp. 21368-21381, 2017.

[4] Fardila M. Zaihidee, Saad Mekhilef and Marizan Mubin, "Application of Fractional Order Sliding Mode Control for Speed Control of Permanent Magnet Synchronous Motor", *IEEE Access*, vol. 7, pp. 101765-101774, 2019.

[5] Peng Gao, Guangming Zhang, Huimin Ouyang and Lei Mei," An Adaptive Super Twisting Nonlinear Fractional Order PID Sliding Mode Control of Permanent Magnet Synchronous Motor Speed Regulation System Based on Extended State Observer", *IEEE Access*, vol. 8, pp. 53498-53510, 2020.

[6] Wei Liu, Siyi Chen and Huixian Huang, "Adaptive Nonsingular Fast Terminal Sliding Mode Control for Permanent Magnet Synchronous Motor Based on Disturbance Observer", *IEEE Access*, vol. 7, pp. 153791-101798, 2019.

[7] Xudong Liu, Haisheng Yu, Jinpeng Yu and Lin Zhao," Combined Speed and Current Terminal Sliding Mode Control with Nonlinear Disturbance Observer for PMSM Drive", *IEEE Access*, vol. 6, pp. 29594-29601, 2018.

[8]   Taochang Li, Yijian Zhao and Limin Hou," Adaptive Sliding Mode Control with Disturbance Observer for Speed Regulation System of Permanent Magnet Synchronous Motor", *IEEE Access*, vol. 11, 17021-17030, 2023.

[9]   Vijayakumar Gali, Nitin Gupta and R.A. Gupta, "Experimental investigations on multitudinal sliding mode Controller-based interleaved shunt APF to mitigate shoot-through and PQ problems under distorted supply voltage conditions", *International Transactions on Electrical Energy Systems*, vol. 29, no.1, pp.1-23, 2019.

[10] C. Evangelista, P. Puleston, F. Valenciaga and L. Fridman," Lyapunov Designed Super-Twisting Sliding Mode Control for Wind Energy Conversion Optimization", *IEEE Transactions on Industrial Electronics*, vol. 60, no. 2, 538–545, Feb. 2013.

[11] Emmanuel Cruz-Zavala, Jaime A. Moreno, and Leonid M. Fridman," Adaptive Gains Super-Twisting Algorithm for Systems with Growing Perturbations", Preprints of the 18th IFAC World Congress, Milano (Italy), pp. 3039-3044, 2011.

[12] Kai Liao, Yan Xu, and Hai Zhou, "A robust damping controller for DFIG based on Variable-gain Sliding Mode and Kalman Filter Disturbance Observer", Electrical Power and Energy Systems, vol. 107, pp. 569–576, 2019.

[13] A. Benamor, M.T. Benchouia, K. Srairi and M.E.H. Benbouzid," A novel rooted tree optimization apply in the high order sliding mode control using super-twisting algorithm based on DTC scheme for DFIG", *Electrical Power and Energy Systems*, vol. 108, pp. 293–302, 2019.

[14] Sadegh Ebrahimkhani, "Robust fractional order sliding mode control of doubly-fed induction generator (DFIG) based wind turbines", *ISA Transactions*, vol. 63, pp. 343–354, 2016.

[15] Hamza Afghoul, Fateh Krim, Badreddine Babes, Antar Beddar, Abbas Kihel, "Design and real time implementation of sliding mode supervised fractional controller for wind energy conversion system under sever working conditions", *Energy Conversion and Management*, vol. 167, pp. 91–101, 2018.

[16] Tomasz Pajchrowski; Krzysztof Zawirski; Krzysztof Nowopolski," Neural Speed Controller Trained Online by Means of Modified RPROP Algorithm", *IEEE Transactions on Industrial Informatics*, vol. 11, no. 2, pp. 560-568, April 2015.

[17] Xiao Sun, Martin H. L. Chow, Frank H. F. Leun, Dehong Xu, Yousheng Wang, and Yim-Shu Lee, "Analogue Implementation of a Neural Network Controller for UPS Inverter Applications", *IEEE Transactions on Power Electronics*, vol. 17, no. 3, pp. 305-313, May 2002.

[18] Cetin Elmas, Oguz Ustun and Hasan H. Sayan, "A neuro-fuzzy controller for speed control of a permanent magnet synchronous motor drive", *Expert Systems with Applications*, vol. 34, pp. 657–664, 2008.

[19] Heng Deng, Dipti Srinivasan and Ramesh Oruganti, "A B-spline network based neural controller for power electronic applications", *Neurocomputing*, vol. 73, pp. 593-601, 2010.

[20] Syed Abdul Rahman Kashif, Muhammad Asghar Saqib and Saba Zia," Implementing the induction-motor drive with four-switch inverter: An application of neural networks", *Expert Systems with Applications*, vol. 38, pp. 11137–11148, 2011.

[21] Young Bae Kong, Min Goo Hur, Eun Je Lee, Jeong Hoon Park, Yong Dae Park, and Seung Dae Yang, "Predictive ion source control using artificial neural network for RFT-30 cyclotron", *Nuclear Instruments and Methods in Physics Research A*, vol. 806, pp. 55-60, 2016.

[22] B. M. Vinagre, I. Podlubny, A. Hern´andez, V. Feliu," Some Approximations of Fractional Order Operators used in Control Theory and Applications", *Fractional Calculus and Applied Analysis*, vol. 3, no. 3, pp. 231–248, 2000.

[23] Y. Q. Chen and B. M. Vinagre," A New IIR-Type Digital Fractional Order Differentiator", *Signal Processing*, vol. 83, no. 11, pp. 2359-2365, Nov. 2003.

[24] Y. Q. Chen and K. L. Moore," Discretization Schemes for Fractional-Order Differentiators and

Integrators", *IEEE Transactions on Circuits and Systems - I: Fundamental Theory and Applications*, vol. 49, no. 3, pp. 363–367, Mar. 2002.

[25] Ivo Petras," Fractional Order Feedback Control of a DC Motor", *Journal of Electrical Engineering*, vol. 60, no. 3, pp. 117–128, 2009.

[26] ANDRZEJ RUSZEWSKI, ANDRZEJ SOBOLEWSKI, "Position control of DC motor using fractional order controller", *Archives of Electrical Engineering*, vol. 62, no. 3, pp. 505-516, 2013.

[27] Ashraf Hagras," Adaptive fractional order sliding mode speed and current control for switched reluctance motor", *Acta Polytechnica Hungarica*, vol. 19, no. 5, pp. 85-106, 2022.

[28] N. V. Uma Maheswari, L. J. Sahaya Shanthi, "Simulation study of ANFIS controller for sensorless induction motor drives at low speeds" *Journal of Electrical Engineering*, vol. 19, no. 1, pp. 488-495, 2019.

[29] N.V. Uma Maheswari, L. Jessi Sahaya Shanthi, "Neural network-based MRAS for sensorless induction motor drives to improve performance at low speeds", *Journal of Electrical Engineering*, vol. 18, no. 2, pp. 464 -471, 2018.

[30] Hicham Chaoui, Mehdy Khayamy, Okezie Okoye, "MTPA based operation point speed tracking for PMSM drives without explicit current regulation", *Electric Power Systems Research*, vol. 151, pp. 125–135, 2017.

[31] Muhammad Usama and Jaehong Kim," Improved Self-Sensing Speed Control of IPMSM Drive Based on Cascaded Nonlinear Control*", Energies*, 2021, pp. 1-22.

_____

مقارنة الأداء بين المتحكم التناسبى الكاملى القائم على الشبكات العصبية ومتحكم النمط المنزلق الجزئي للتحكم في سرعة المحرك المتزامن ذو المغناطيس الدائم الداخلي بدون حساس

الملخص :

يقارن هذا البحث بين أداء المتحكم التناسبى التكاملى باستخدام الشبكات العصبية وأداء متحكم النمط المنزلق الجزئى للتحكم فى سرعة المحرك المتزامن ذو المغناطيس الدائم الداخلى بدون حساس. اقترح البحث طريقة جديدة للتحكم في السرعة بدون حساس للمتحكم التناسبى التكاملى القائم على الشبكات العصبية بناءً على التعلم غير المتصل باستخدام جدول البحث الذي تم الحصول عليه من تحليل المتحكم التناسبى التكاملى. تم تصميم متحكم النمط المنزلق الجزئى وتحليله وتم ضمان استقراره باستخدام نظرية استقرار Lyapunov للتحقق من أدائه العالى. تقترح هذه الورقة مراقب سرعة جديد كمرشح تمرير منخفض لتيارات المحرك وعزم الحمل في المجال الزمني لزيادة موثوقية نظام المسار المغلق. أثبتت نتائج المحاكاة باستخدام MATLAB/SIMULINK الأداء المحسن لوحدتي التحكم والأداء القوي لمتحكم النمط المنزلق الجزئى مقارنة بالمتحكم التناسبى التكاملى باستخدام الشبكات العصبية فى نطاقات كبيرة من تغير معاملات المحرك واضطرابات الحمل الخارجية في مخطط التحكم باستخدام المجال الموجه. تم تقديم دراسة تحليلية لتأثير عامل التفاضل الجزئي لإظهار أنه مع انخفاض قيمته، يتم تحسين أداء الحالة العابرة والثابتة للمحرك.